Efficient transient noise analysis of non-periodic mixed analogue/digital circuits

Matteo Biggio[2], Federico Bizzarri[1], Angelo Brambilla[1], Marco Storace[2]

[1]Dipartimento di Elettronica, Informazione e Bioingegneria, Politecnico di Milano, P.zza Leonardo da Vinci, n. 32, I-20133 Milano, Italy
[2]DITEN, University of Genoa, Via Opera Pia 11a, I-16145 Genova, Italy
E-mail: angelo.brambilla@polimi.it

1 Introduction

During the last two decades, radio frequency (RF) circuits have conquered a large portion of the electronic market and 'mobile' devices are largely used everyday. One of the key aspects in designing a 'good quality' RF device is reduction of noise. Effects of noise have been deeply studied from different points of view and new numerical algorithms to efficiently simulate noise in electronic circuits have been developed and made available in commercial circuit simulators. When applicable, a successful method to simulate noise is based on two sequential steps. The first determines the periodic steady-state large-signal solution (e.g. through shooting or harmonic balance methods [1]) of the circuit with the noise sources turned off. The second linearises the equations describing the circuit around the periodic orbit, thus leading to a linear time-varying system (variational model) [2]. Noise sources are then turned on and their effects are transferred to the circuit output.

In commercial simulators, such as, for example, SPECTRE™ by CADENCE, this analysis is referred to as periodic noise analysis (PNOISE) [3–5]. However, there are at least two cases (each one violating one of the assumptions for the two steps) in which this approach cannot be successfully applied.

First, modern RF circuits are made up of both 'analogue' blocks, modelled through differential algebraic equations (DAEs), and 'digital' blocks, modelled through boolean functions and maps or behavioural elements that generate discontinuous signals. This mixed analogue/digital approach is dictated by the fact that these circuits are usually made up of a very-large number of elements mainly located in their digital part, thus making a transistor-level simulation (i.e. as analogue circuits described by DAEs) often unfeasible. Mixed analogue/digital circuits are described by non-smooth systems and consequently their variational models are not defined. In principle, it is thus not possible to resort to PNOISE to determine the effects of noise sources. Second, there are circuits that do not admit a steady-state solution, for example, a fractional $\Delta\Sigma$ phase-locked loop (PLL) with dithering or pulled oscillators [6]. In both cases, one has to resort to time-domain (large-signal) noise analysis, where contributions by noise sources to the circuit electrical variables are computed during the numerical solution, without need for a periodic steady-state. At the end of this simulation, waveforms can be processed to extract the power spectral density (PSD) of noise.

This approach has three main drawbacks. The first one is the numerical *noise floor*, which can hide the effects of the noise sources. This prevents the successful application of time-domain noise analysis to low-noise circuits, that are obviously the real target of the RF design. This point is discussed in [7] by focusing on a basic oscillator example to show the limits of circuit simulators because of numerical tolerances of the used iterative algorithms (see also [8, 9]). The 'random walk' of the *large* signal solution caused by numerical errors constitutes the *noise floor*, and characterises the relative accuracy of the simulator with respect to the effect of noise sources; noise sources leading to effects below the noise floor are completely hidden.

The second drawback is the relative numerical inaccuracy of the large-signal simulation with respect to variational approaches, which cannot be directly applied to non-continuous vector fields.

The third (more involved) phenomenon is concerned with the fact that – in circuits not admitting a periodic steady-state – noise PSD cannot be accurately determined by resorting to standard fast Fourier transform (FFT) methods. A common approach consists in determining the time sequence of threshold crossings of a noisy large-signal solution. This sequence is then post-processed to compute the Welch's periodogram [10]. However, linear multi-step methods used to transform the DAEs modelling the analogue part of the circuit into non-linear algebraic equations contribute to the noise floor of simulators through *time warping*, that is, they distort time and thus corrupt accuracy of the threshold crossing time instants [8]. This can make useless the adoption of the Welch's periodogram to avoid biasing of standard FFT.

In summary, on the one hand, to analyse the effects of noise sources on a mixed analogue/digital circuit, a time-domain noise analysis tool is needed to compute the noise PSD, since PNOISE is not applicable; on the other hand, the noise floor of the simulator introduced by the time-domain large-signal algorithm can almost completely hide noise effects of the circuit. A variational approach would allow to reduce this problem since, in general, the numerical accuracy of a DAE solution is relative to its order of magnitude, but it must be extended to switching DAEs modelling mixed analogue/digital circuits not admitting a periodic solution.

This paper is concerned with the practical problem of simulating noise in mixed analogue/digital circuits with behavioural description of some digital parts. To this end, three ingredients (already known individually but, at the best of the authors' knowledge, never combined to this end) are 'cooked' together to solve the above cited drawbacks. The *saltation matrix* allows extending the *variational model* to mixed analogue/digital circuits and then reducing the noise floor [11–14]. To extract the PSD of noise, the Thomson's multitaper method (MTM) is used, which – with respect to Welch's periodogram – has the advantage of a lower biasing in the estimation, because of the use of orthogonal tapers. Noise is characterised through one simulation run only, thus gaining numerical efficiency without giving up numerical accuracy.

The numerical simulations reported in this paper are validated by experimental measurements on a commercial fractional ΔΣ PLL.

2 A glimpse to the noise floor: warping

One of the main contributions to the noise floor is because of the *warping* of the solution introduced by linear multi-step integration methods [8, 15], largely used in circuit simulators [9]. The time warping effect consists in a modification of the period of an oscillator because of the finite integration time step used in linear multi-step integration methods [15]. To show how warping affects time-domain noise simulation methods, consider the relaxation oscillator shown in Fig. 1. Assume the S switch closed, so that the voltage-controlled current source injects a current $\mathrm{Ao} = z/R$. The circuit is modelled as an impact system described by: two ordinary differential equations (ODEs)

$$\begin{cases} C\dot{x}(t) + \dfrac{1}{R}(x(t) - z(t)) = 0, \\ \dot{z}(t) = 0 \end{cases} \tag{1}$$

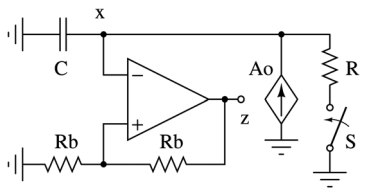

Fig. 1 *Schematic representation of the relaxation oscillator*

Two different working configurations are considered; the former has the switch S closed and the controlled source injects the current $\mathrm{Ao} = z/R$. The latter has S open and the capacitor C charges/discharges trough the voltage-controlled current source Ao (see text)

the impact condition defined by the manifold

$$\kappa(x, z) = x - t\frac{z}{2} = 0 \tag{2}$$

and the reset rule [16]

$$z(t^+) = -z(t^-) \tag{3}$$

Assume to start the numerical solution of (1) from the initial conditions $x_0 = -z_o$ and z_o. The voltage $x(t)$ across C oscillates between the two values $-z_o/2$ and $+z_o/2$. The $T/2$ working period of this oscillator is determined by the time interval between two consecutive applications of the map (3). By assuming that circuit elements are *noiseless* and computing the time instants of map application, the standard deviation of the time intervals between two consecutive map evaluations is expected to be $\sigma = 0$, that is, the oscillator is not affected by jitter and the PSD of phase noise is null [17]. This expectation is wrong, since warping introduces variations in the time instants of map application. These variations depend on the integration time step and, paradoxically, by varying it from cycle to cycle to accurately obtain the time instant of map application, the value of the working period of the relaxation oscillator changes. This results in $\sigma \neq 0$ and in an increased noise floor of the simulator, which can be 'confused' with oscillator jitter.

The oscillator shown in Fig. 1 was simulated with SPECTRE™ by CADENCE by performing a time-domain noise analysis. All elements were *noiseless*, therefore in principle the result should not be affected by any noise.

The comparator was implemented as a VERILOGA module and the $\kappa(x, z)$ manifold crossings were accurately computed by resorting to the 'cross()' function with a time accuracy of 1 ns; the working period of the oscillator is some seconds and more than 30 000 manifold crossings were computed. The obtained variance $\sigma^2 = 1.3859 \times 10^{-8}$ clearly points out that the oscillator is affected by 'artificial' jitter (warping), well above the 'cross()' function accuracy.

When the switch S in the circuit of Fig. 1 is open, C is charged by a constant current. Since linear multi-step integration methods are of order 1 or larger, they *exactly* integrate this current. In other words, they do not introduce any warping when the simulator varies the integration time step to accurately meet the time instant of the manifold crossing. The same simulation performed by using SPECTRE resulted in $\sigma^2 = 1.3851 \times 10^{-12}$, which is well below the previous value.

To further corroborate the above statements, the 'phase noise' spectrum was computed by resorting to the PSD

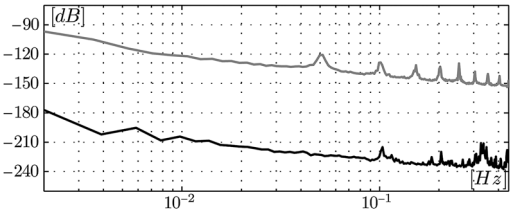

Fig. 2 *Phase noise PSDs of the oscillator shown in Fig. 1 computed by the psd function of MATLAB*

Time samples from which we derived PSDs were computed through a time-domain noise simulation by SPECTRE. Peaks reveal the presence of a periodicity in the choice of the integration time step from working cycle to working cycle of the oscillator. Gray curve: S closed; black curve: S open. *x*-axis: frequency offset from the fundamental, *y*-axis: dB [W/Hz]

estimate of a signal using Welch's overlapped segment method available in MATLAB [10]. This is a standard procedure adopted by RF circuit designers. The obtained PSDs with S closed (i.e. with time warping) and open (i.e. without time warping) are shown in Fig. 2. It can be easily appreciated that there is a drop of about 90 dB in the noise floor of the simulator when warping effects are removed.

In conclusion, the noise floor of standard time-domain noise analysis can strongly limit its applicability, since warping can easily hide effects because of low-noise sources.

We remark that $\sigma \neq 0$ with S open since other numerical noise sources contribute to the final results. By simulating the circuit of Fig. 1 with the approach presented in the next sections, the PSD at node z was 0, being the circuit noiseless. These results are omitted from Fig. 2 since they correspond to $-\infty$ dB.

3 The method

This section describes the main ingredients of the proposed method, which allows to reduce the noise floor because of both warping (since the method is not based on zero-crossing detection) and numerical inaccuracies (owing to its variational nature). For the interested reader, the modified nodal analysis (MNA) formulation is briefly summarised in Appendix 1, together with the related variational model. The derivation of the linear time-varying stochastic equations modelling the effects of *small-amplitude* noise sources is sketched. It is shown how the saltation matrix can be used to extend the variational model of the circuit to the transient noise simulation of mixed-signal circuits [11]. The PSDs of the noisy electrical variables are then computed by resorting to the Thomson's MTM, since it is less biased than the Welch's periodogram, thus allowing to resort to a single simulation run.

3.1 Stochastic variational model

In [11] the variational model (see Appendix 1) has been used to implement a noise simulator in time-domain, which is able to produce the noise variance and correlation of circuit variables as a function of time. In principle, all circuits that can be simulated by the transient analysis in a circuit simulator can be handled. The basic idea is that the homogeneous linear time-varying differential equation (see Appendix 1, (11)) is forced by a vector $\boldsymbol{\eta}$ of P standard white Gaussian stochastic processes [18], modelling the P 'small amplitude' noise sources that are assumed to affect the original circuit. The circuit stochastic variational model is then

$$\dot{\boldsymbol{\xi}}(t) = \boldsymbol{J}(t)\boldsymbol{\xi}(t) + \boldsymbol{D}(t)\boldsymbol{\eta}(t) \tag{4}$$

where $\boldsymbol{D}(t) \in \mathbb{R}^{S\times P}$ is a time-varying matrix reflecting the contribution of $\boldsymbol{\eta}$ on each one of the S equations of the variational model. Equation (4) can be rewritten in differential form as

$$\mathrm{d}\boldsymbol{\xi}_t = \boldsymbol{J}(t)\boldsymbol{\xi}_t \mathrm{d}t + \boldsymbol{D}(t)\underbrace{\boldsymbol{\eta}_t \mathrm{d}t}_{\mathrm{d}\boldsymbol{W}_t}, \quad \boldsymbol{\xi}_{t_0} = \boldsymbol{c} \tag{5}$$

where $\boldsymbol{\xi}_t$ is a random variable defining the stochastic process $\boldsymbol{\xi} = \{\boldsymbol{\xi}_t, t > t_0\}$ and $\boldsymbol{W} = \{\boldsymbol{W}_t, t > t_0\}$ is a Wiener process [18]. Since (5) is a stochastic differential equation (SDE) in a 'narrow sense', (In general a linear SDE takes the form $\mathrm{d}\boldsymbol{\xi}_t = \alpha(t, \boldsymbol{\xi}_t)\mathrm{d}t + \beta(t, \boldsymbol{\xi}_t)\mathrm{d}\boldsymbol{W}_t$, where $\alpha(t, \boldsymbol{\xi}_t) = \boldsymbol{a}_1(t)\boldsymbol{\xi}_t + \boldsymbol{a}_2(t)$ and $\beta(t, \boldsymbol{\xi}_t) = \boldsymbol{b}_1(t)\boldsymbol{\xi}_t + \boldsymbol{b}_2(t)$. Whenever $\boldsymbol{b}_1(t) = \boldsymbol{0}$ the SDE is said to be linear in a 'narrow sense'.) its solution can be derived as [19]

$$\boldsymbol{\xi}_t = \boldsymbol{\Phi}_{\boldsymbol{v}_0}(t, t_0)\boldsymbol{c} + \int_{t_0}^{t} \underbrace{\boldsymbol{\Phi}_{\boldsymbol{v}(\tau)}(t, \tau)\boldsymbol{D}(\tau)}_{\boldsymbol{F}(\tau)} \mathrm{d}\boldsymbol{W}_\tau \tag{6}$$

where $\boldsymbol{v}_0 = \boldsymbol{v}(t_0)$ and $\boldsymbol{\Phi}_{\boldsymbol{v}(\tau)}(t, \tau)$ is the fundamental transition matrix (see Appendix 1) computed from τ to t along a large-signal trajectory $\boldsymbol{v}$ originating from $\boldsymbol{v}(\tau)$ at τ. The 'integral' in (6) is a vector whose entries are sums of stochastic integrals where a deterministic function is integrated with respect to a Wiener process. Equation (6) is a stochastic process representing the evolution (at first order in the noise intensity) of a small perturbation relative to the noise-free large-signal solution.

3.2 From analogue to mixed-signal circuits: the saltation matrix

The main limitation of the simulator presented in [11], apart from its computational cost, is that $\boldsymbol{\Phi}_{\boldsymbol{v}_0}(t, t_0)$ must exist for any $t \geq t_0$ and in general this is not true for mixed-signal circuits. Indeed, to guarantee the existence of $\boldsymbol{\Phi}_{\boldsymbol{v}_0}(t, t_0)$, it is mandatory that $\boldsymbol{J}(t)$ is continuous and this is not the case for mixed-signal circuits.

In [12] a unified simulation framework was presented, which allows to manage mixed-signal circuits described by an index-1 DAE. In particular it was shown that, by resorting to the saltation matrix linear operator [20], it is possible to extend to this extremely large class of circuits several techniques commonly employed to study smooth analogue circuits [21].

To understand how this linear operator is defined and how it must be used, in the following we assume to deal with an ODE (A complete description of the DAE case can be found in [12].).

Consider the $\boldsymbol{v}(t)$ reference trajectory shown in Fig. 3 that, starting from $\boldsymbol{v}_0$ at $t = t_0$, hits the $\kappa(\boldsymbol{v}, t) = 0$ time varying manifold at $\boldsymbol{v}_1$ for $t = t_1$. This manifold divides the state space in two regions where the dynamics is ruled by two different vector fields, say $\boldsymbol{f}_l(\boldsymbol{v}, t)$ and $\boldsymbol{f}_r(\boldsymbol{v}, t)$ on the left and on the right of the manifold, respectively. By perturbing the initial point by $\Delta\boldsymbol{v}_0$, the perturbed trajectory hits the manifold at $\boldsymbol{v}_2$ with time delay Δt with respect to the unperturbed one, since for $t = t_1$ it is still in $\boldsymbol{v}_4$. In Δt the reference trajectory evolves from $\boldsymbol{v}_1$ to $\boldsymbol{v}_3$ with the vector

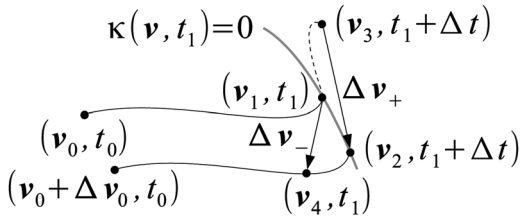

Fig. 3 *Example of a trajectory hitting a manifold*

field $\boldsymbol{f}_r(\boldsymbol{v}, t)$. It can be shown that there exists a matrix $\mathcal{S} \in \mathbb{R}^{N\times N}$ such that, at first order, $\boldsymbol{v}_2 - \boldsymbol{v}_3 = \Delta\boldsymbol{v}_+ = \mathcal{S}\Delta\boldsymbol{v}_- = \mathcal{S}(\boldsymbol{v}_4 - \boldsymbol{v}_1)$. In the literature, $\mathcal{S}$ is referred to as 'saltation matrix'. If one is interested in evaluating the fundamental matrix of the system from $\boldsymbol{v}_0$ to $\boldsymbol{v}_3$, $\mathcal{S}$ is necessary to match $\boldsymbol{\Phi}_{\boldsymbol{v}_0}$ at the discontinuity boundary (where the Jacobian of the vector field is not defined), that is, $\boldsymbol{\Phi}_{\boldsymbol{v}_0}(t_1 + \Delta t, t_0) = \boldsymbol{\Phi}_{\boldsymbol{v}_1}(t_1 + \Delta t, t_1)\mathcal{S}\boldsymbol{\Phi}_{\boldsymbol{v}_0}(t_1, t_0)$. The explicit formula for $\mathcal{S}$ (see [20]), which is defined provided that the reference trajectory hits the manifold transversally, is

$$\mathcal{S} = \boldsymbol{I}_N + \frac{\left[\boldsymbol{f}_l(\boldsymbol{v}_1, t_1) - \boldsymbol{f}_r(\boldsymbol{v}_1, t_1)\right]\boldsymbol{\eta}_v^{\mathrm{T}}}{\boldsymbol{\eta}_v^{\mathrm{T}}\boldsymbol{f}_l(\boldsymbol{v}_1, t_1) + \boldsymbol{\eta}_t} \tag{7}$$

where $\boldsymbol{\eta}_v^{\mathrm{T}} = \nabla_{\boldsymbol{v}}\kappa(\boldsymbol{v}, t)\big|_{\boldsymbol{v}_1,t_1}$, $\boldsymbol{\eta}_t^{\mathrm{T}} = \left.\dfrac{\partial\kappa(\boldsymbol{v}, t)}{\partial t}\right|_{\boldsymbol{v}_1,t_1}$, and $\boldsymbol{I}_N$ is the $N \times N$ unit matrix.

The saltation matrix can be basically viewed as a 'correction factor' matching the fundamental matrix before and after each discontinuity event occurring at time t_k. In other words, it gives $\boldsymbol{\Phi}_{\boldsymbol{v}_0}(t_k^+, t_0)$ in terms of $\boldsymbol{\Phi}_{\boldsymbol{v}_0}(t_k^-, t_0)$ as

$$\boldsymbol{\Phi}_{\boldsymbol{v}_0}(t_k^+, t_0) = \mathcal{S}_k\boldsymbol{\Phi}_{\boldsymbol{v}_0}(t_k^-, t_0) \tag{8}$$

The saltation matrix is well known when dealing with piecewise-smooth ODEs, and has been successfully applied in the modelling and simulation of mixed analogue/digital circuits [13, 14].

It is important to point out that the insertion of saltation matrices in the evolution of $\boldsymbol{\Phi}_{\boldsymbol{v}_0}(t, t_0)$ makes its entries exhibit stepwise discontinuities. This is not an issue in defining the stochastic integrals in (6), since the deterministic functions involved need just to be square-integrable [22]. To summarise, when implementing the extended method to perform transient noise analysis of mixed analogue/digital circuits, during the large-signal time-domain analysis of the noiseless circuit, the matrix $\boldsymbol{\Phi}_{\boldsymbol{v}_0}(t, t_0)$ is computed by taking also into account crossings that cause switching of the vector field or resetting of state variables. Each time this happens, a proper saltation matrix is computed and inserted in the matrix product chain that leads to $\boldsymbol{\Phi}_{\boldsymbol{v}_0}(t, t_0)$, to regularise the variational model.

3.3 Phase noise spectrum estimation: the MTM

One of the most widely employed methods for estimating the phase noise (or jitter) PSD is based on the computation of the threshold-crossings of a circuit electrical variable. The Welch's periodogram is usually applied to the time-series of the differences between two consecutive threshold-crossings [10, 23]. In large-signal time-domain approaches, this method suffers from inaccuracies, mainly because of the time-warping effect described in Section 2. Furthermore, if the variational model is used, the threshold-crossing technique cannot be used, since, when the variational solution is added to the noiseless large-signal solution, numerical errors can hide the effects of noise. To overcome these problems, the following method is employed. During the time-domain analysis, (6) is computed on a mesh $\mathcal{T}$ of evenly-spaced time points. The resulting set of samples, representing a *single* realisation of the stochastic process modelling additive noise effects in the circuit, is hence processed by Thomson's MTM [24]. By working on the $\mathcal{T}$ mesh, MTM estimates the PSD of the stochastic solution using multiple orthogonal windows of this single realisation, thus avoiding large biasing and hence the need of performing several simulations. The variational problem (12) is solved by adopting a variable step-size method controlling the integration time step in order make available the accurate $\boldsymbol{\Phi}_{\boldsymbol{v}_0}(t, t_0)$ fundamental matrix at the time points belonging to $\mathcal{T}$.

3.4 Noise sources

In circuit simulators, complex elements (such as MOSFETs) are implemented through 'built-in' sub-circuits. Generally speaking, each element in these sub-circuits (e.g. the parasitic gate, source and drain resistors and the channel of MOSFETs) may generate coloured noise, thus requiring a ladder RC filter to shape the output of a corresponding white noise generator [25]. This increases the number of circuit equations to be simultaneously solved. In this paper, coloured noise (in particular f^{α} noise with $-2 < \alpha < 0$) generation relies on the approach proposed and developed in [25, 26], but the colouring ladder RC analogue filter required by each coloured noise source is replaced by a lead-lag digital filter. This filter is usually made up of no more than $Q = 15$ sections depending on the required bandwidth of the corresponding noise source. In case a coloured noise source is modulated by the current flowing in a time-varying device, the output of the digital filter is modulated accordingly. From a numerical standpoint, this approach requires that each flicker noise generator adds a number Q of 'digital' state variables. The main advantage is that they are not handled and solved together with the circuit electrical variables, thus increasing the numerical efficiency. Digital filters are automatically initialised by the simulator before starting the time-domain noise analysis, as described in [27]. In the proposed implementation, during time domain noise simulations the output of these bank of coloured noise generators (potentially one for each element constituting the built-in sub-circuits) is 'automatically' sampled at each time point of $\mathcal{T}$, thus the final user does not look after that. This was done by extending the code of the built-in models handled in our simulator, such as, for example, the well-known BSIM3 and BSIM4 MOSFET models.

4 Results

The proposed method is applied to a commercial real-world device, a fractional PLL, modelled as mixed analogue/digital system, and the obtained results are compared with experimental data.

4.1 Experimental setup

The experiments were conducted by using the PLL implemented on the UG-369 evaluation board by ANALOG DEVICES, that mounts the AD4151 PLL and the ROS-1800+ voltage controlled oscillator (VCO). The

frequency measurements were performed through the spectrum analyser E4440 of AGILENT TECHNOLOGIES. The time measurements were obtained through the oscilloscope LeCroy Waverunner LT584. The device was configured as a fractional PLL characterised by a VCO working at 1775.2 MHz, with a reference frequency of 25 MHz, and a frequency ratio $N = 70 + (26/125)$, where the fractional part is obtained by means of a 12-bit ΔΣ modulator.

4.2 PLL and VCO models

The block schematic of the circuit used to model the PLL is shown in Fig. 4. The ΔΣ fractional divider was implemented as a digital block through the VERILOG language. As reported in the data-sheet, the MASH ΔΣ modulator is characterised by 12 bits, the accumulator size is 125 (i.e. it generates a carry signal when its content exceeds 125), and the input value k (see Fig. 4) is equal to 26. The N division factor sets to an average value of 70.208, corresponding to an average working frequency of the VCO of 1755.2 MHz. A detailed description of the blocks composing the PLL and of the parameter values can be found in [28].

The VCO was modelled as a 'polar oscillator' that generates a pure sinusoidal waveform [29], taking into account its phase noise and its input-output characteristic. This choice was dictated by the fact that the netlist and models of the VCO and PLL were not available and thus they were substituted by macro-models. More specifically the VCO output noise was simulated by an equivalent unique noise source whose PSD was fitted to experimental measurements. The independent voltage source η_ϕ connected to the VCO shown in Fig. 4 does this by injecting equivalent white Gaussian noise, that is, an equivalent Gaussian random number generator was automatically linked to this element by the simulator. To characterise noise, we resorted to the shooting and PNOISE analyses of SPECTRE, which are applicable in this case since the oscillator admits a periodic steady-state solution. By turning η_ϕ on and varying its magnitude, the root-mean-square error (RMSE) between the measured PSD

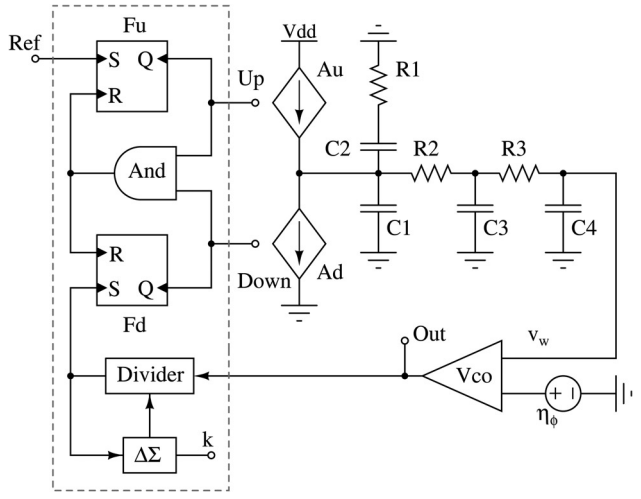

Fig. 4 *Schematic implementing the model of the fractional commercial PLL AD4151 used as test bench*

Blocks inside the dashed box are modelled as digital elements through the verilog language. The other elements are modelled as analogue devices. Fixed parameters: $C1 = 6.8$ nF, $C2 = 120$ nF, $C3 = C4 = 4.7$ nF, $R1 = 120\ \Omega$, $R2 = R3 = 75\ \Omega$, Au = Ad = 2.25 mA, $K_{vco} = 47$ MHz, $f_{ref} = 25$ MHz

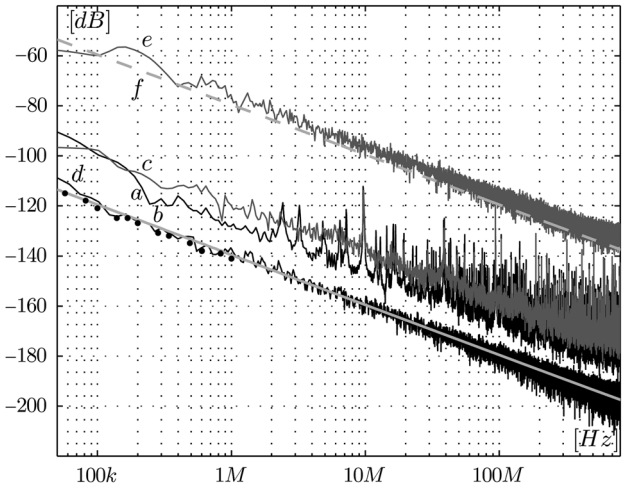

Fig. 5 *PSD of the ros-1800 + VCO computed by the time-domain noise analysis of SPECTRE and by the proposed approach*

Black dotted curve corresponds to the measured PSD; the almost overlapping grey curve labeled as 'b' is the result from PNOISE after having fitted the VCO parameters. Curve labeled as 'a' is the noise floor of SPECTRE which is above the measured PSD. See the main text for a description of the other curves

of noise (black dotted curve in Fig. 5) and the simulated one obtained by PNOISE (grey solid curve 'b') was minimised. A PSD of −168 dBm led to a good fitting.

4.3 VCO simulation

Several simulations were performed, whose results are shown in Fig. 5 (The circuit simulator PAN, developed by the authors and used derive the reported results, is available at the URL: http://brambilla.ws.dei.polimi.it.). A first time-domain noise analysis was carried out with SPECTRE by setting the noisefmax = 3 GHz transient analysis option – since the VCO generates a pure sinusoid and thus it does not show harmonics – and turning off η_ϕ to determine the noise floor. The noisefmax = 3 GHz statement turns on random number generators and injection of noise in the circuit and defines their bandwidth. More than 16000 threshold crossings were computed and then a Welch's PSD was performed. The obtained PSD of the noise floor is the black solid curve '*a*', to be compared with the experimental one (black dotted curve). The simulated noise floor is at least 12 dB 'higher' than the measured phase noise. This means that the time-domain noise analysis of SPECTRE is not reliable in this case. The VCO phase noise was measured till 1 MHz since this is the usual upper limit of the offset frequency in practical applications, as reported also on the data-sheet of the VCO. Simulated curves were continued up to about 1 GHz which is consistent with the value of noisefmax.

To further evidence the inaccuracy of SPECTRE, a second time-domain noise analysis was performed with η_ϕ on (the same command syntax as for SPECTRE was implemented in our simulator); the corresponding result is the grey curve '*c*'. As expected, it is above the noise floor, with an error of about +20 dB.

A noise analysis was then carried out by using the proposed approach (using the Thomson's MTM for PSD estimation); the result is the black curve '*d*', which exhibits a very good match with respect to the experimental dotted curve.

As a further check, the magnitude of η_{db} was artificially increased (so that the expected result by SPECTRE should be well above the noise floor), a time-domain noise analysis was performed with SPECTRE, the PSD was computed through MTM and finally the obtained result (grey curve '*e*') was compared with the corresponding one (dashed grey curve '*f*') by PNOISE. The good matching between the two results is evident.

4.4 PLL simulation

A time-domain simulation with the noise source turned off (to bring $v_w(t)$ close to its average value) and a time-domain noise simulation with the proposed approach were performed for 200 μs. This corresponds to simulate about 3 50 000 working cycles of the VCO and ensures an offset frequency of a few kHz from the fundamental at 1755.2 MHz in the PSD of the PLL noise. The noisy time-domain waveform obtained with the proposed approach was processed by the Thomson's MTM and the resulting PSD is shown in Fig. 6 (black curve) [24]. In the same figure, the experimental measure (light grey curve) is also shown. A good match between the two curves can be appreciated; the error in the PLL bandwidth (25 kHz) is less than 1 dB. For frequency offsets larger than 1 MHz, the experimental PSD sets to the noise floor of the spectrum analyser, that is about −150 dB. The simulated PSD correctly falls with a slope of −20 dB/dec.

To obtain the results reported in Fig. 6, the total CPU time, for simulation performed on an INTEL I7/2600, 16 byte RAM running LINUX-MINT, was 237 s.

One apparently problematic aspect is that the simulated results in Fig. 6 does not show any spur because of the ΔΣ modulator. In the experimental curve, spurs appear at 200 kHz ($=f_{ref}/125$) and harmonics. We remark that spurs are a large-signal effect, therefore they do not appear in the simulated result. The spectrum analyser does not distinguish among PSD of noise and of spurs and thus shows also the latter. Therefore a large-signal noiseless simulation of the fractional PLL (Of course, we already have the large-signal noiseless simulation of 200 μs, but to appreciate the spurs we need a much longer simulation.) has to be performed to reproduce spurs. This is not trivial, in general, since the simulator can be affected by a large noise floor that can hide spikes because of spurs.

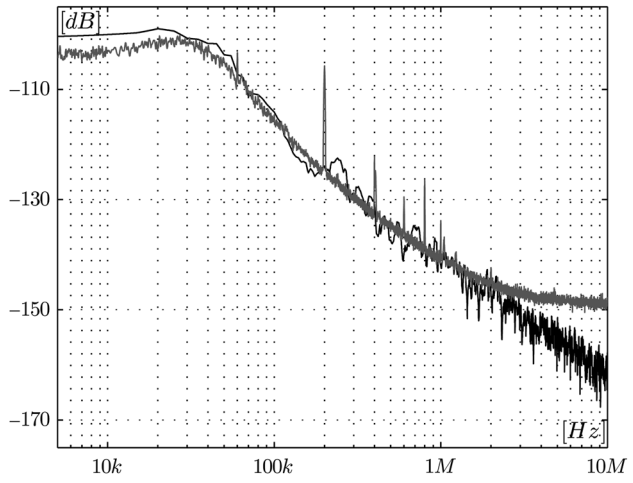

Fig. 6 *Simulated (black curve) and the measured (light gray curve) PSDs of the fractional PLL used as test vehicle*

Average fundamental frequency of the VCO is 1755.2 MHz. The PLL bandwidth is 25 kHz, as reported in the data-sheet. *x*-axis: right offset frequency from the VCO working frequency; *y*-axis: PSDs[W/HZ]

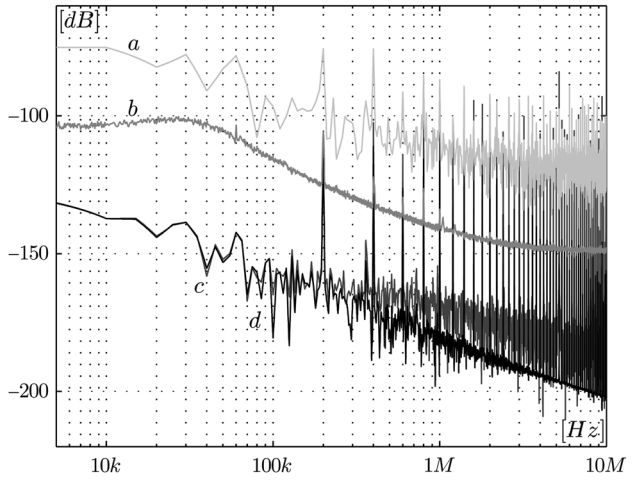

Fig. 7 *Traces are described from the upper to the lowest which corresponds to describe them from the lightest grey to black*

a Large-signal PSD at the output of the VCO
b Measured PSD
c PSD at the output of the charge pump
d PSD at the output of the fourth order filter, that is, at the input of the VCO.
x-axis: right offset frequency from the VCO working frequency; *y*-axis: PSD [W/Hz]

Fig. 7 shows the results of this long-lasting large-signal noiseless simulation. As expected, spikes appear at 200 kHz and at harmonics in the PSD at the output of the charge pump (curve '*c*'). The spikes are attenuated in the PSD at the output of the fourth-order filter (dark grey curve '*d*') that connects the charge pump to the input of the VCO. The noise floor of the simulator can be easily identified and fortunately it is well below the values of the spikes. This does not happen to the PSD at the output of the VCO (curve '*a*'), which is affected by a very large noise floor well above the measured PSD of noise (curve '*b*'). Spikes because of spurs are still visible but their amplitudes are incorrect.

5 Conclusions

In this paper a method was proposed for efficient non-Monte Carlo transient noise analysis of mixed analogue/digital circuits. With respect to the approaches commonly used in commercial simulators, some key ingredients are used: the saltation matrix for handling circuits described by non-smooth vector fields, a variational model for reducing the noise floor effects, and the Thomson's MTM for efficient estimation of the noise spectrum. These features allow reliable noise characterisation by employing only one simulation run, thus considerably reducing the computational cost without affecting the accuracy of the results.

The proposed test bench (a fractional ΔΣ PLL) points out an excellent matching between simulations and experiments for the described method, and, at the same time, shows the limits of widely used commercial simulators.

6 Acknowledgments

The authors thank Mr. Giorgio Carlini for his valuable help in performing the experimental measurements. Work supported by Regione Lombardia and Politecnico di Milano (SPUMA project) and by University of Genoa.

7 References

1 Kundert, K., Sangiovanni-Vincentelli, A.: 'Simulation of nonlinear circuits in the frequency domain', *IEEE Trans. Comput. Aided Des.*, 1986, **CAD-5**, (4), pp. 521–535

2 Traversa, F., Bonani, F.: 'Oscillator noise: a nonlinear perturbative theory including orbital fluctuations and phase-orbital correlation', *IEEE Trans.Circuits Syst. I, Regul. Pap.*, 2011, **58**, (10), pp. 2485–2497

3 Okumura, M., Sugawara, T., Tanimoto, H.: 'An efficient small signal frequency analysis method of nonlinear circuits with two frequency excitations', *IEEE Trans. Comput. Aided Des. Integr. Circuits Syst.*, 1990, **9**, pp. 225–235

4 Brambilla, A., Storti Gajani, G.: 'Computation of all the Floquet eigenfunctions in autonomous circuits', *Int. J. Circuit Theory Appl.*, 2008, **36**, (5–6), pp. 717–737

5 Traversa, F., Bonani, F.: 'Selective determination of floquet quantities for the efficient assessment of limit cycle stability and oscillator noise', *IEEE Trans. Comput. Aided Des. Integr. Circuits Syst.*, 2013, **32**, (2), pp. 313–317

6 Buonomo, A., Lo Schiavo, A.: 'Nonlinear dynamics of divide-by-two injection-locked frequency dividers in locked operation mode', *Int. J. Circuit Theory Appl.*, 2013. [Online]. Available: http://dx.doi.org/10.1002/cta.1888

7 Biggio, M., Bizzarri, F., Brambilla, A., Storace, M.: 'Effects of numerical noise floor on the accuracy of time domain noise analysis in circuit simulators'. IEEE Int. Symp. on Circuits and Systems (ISCAS), 2013, pp. 2694–2697

8 Brambilla, A., Storti-Gajani, G.: 'Frequency warping in time domain circuit simulation', *IEEE Trans. Circuits and Syst. I, Fundam. Theory Appl.*, 2003, **50**, pp. 904–913

9 Vlach, J., Singhal, K.: 'Computer methods for circuit analysis and design' (Van Nostrand Reinhold Company, 1983)

10 Welch, P.: 'The use of fast Fourier transform for the estimation of power spectra: a method based on time averaging over short, modified periodograms', *IEEE Trans. Audio Electroacoust.*, 1967, **15**, (2), pp. 70–73

11 Demir, A., Liu, E., Sangiovanni-Vincentelli, A.: 'Time-domain non-Monte Carlo noise simulation for nonlinear dynamic circuits with arbitrary excitations', *IEEE Trans. Comput. Aided Des. Integr. Circuits Syst.*, 1996, **15**, (5), pp. 493–505

12 Bizzarri, F., Brambilla, A., Storti Gajani, G.: 'Steady state computation and noise analysis of analog mixed signal circuits', *IEEE Trans. Circuits Syst. I, Regul. Pap.*, 2012, **59**, (3), pp. 541–554

13 Bizzarri, F., Brambilla, A., Storti Gajani, G.: 'Extension of the variational equation to analog/digital circuits: numerical and experimental validation', *Int. J. Circuit Theory Appl.*, 2013, **41**, (7), pp. 743–752. [Online]. Available: http://dx.doi.org/10.1002/cta.1864

14 Bizzarri, F., Brambilla, A., Storti Gajani, G.: 'Phase noise simulation in analog mixed signal circuits: an application to pulse energy oscillators', *IEEE Trans. Circuits Syst. II, Express Briefs*, 2011, **58**, (3), pp. 154–158

15 Gear, C.W.: 'Numerical initial value problems in ordinary differential equations' (Prentice-Hall, 1971)

16 Bizzarri, F., Brambilla, A., Gajani, G.S.: 'Lyapunov exponents computation for hybrid neurons', *J. Comput. Neurosci.*, 2013, pp. 1–12

17 Lee, D.: 'Analysis of jitter in phase-locked loops', *IEEE Trans. Circuits Syst. II, Analog Digit. Signal Process.*, 2002, **49**, (11), pp. 704–711

18 Kloeden, P.E., Platen, E.: 'Numerical solution of stochastic differential equations' (Springer-Verlag, 1992)

19 Arnold, L.: 'Stochastic differential equations: theory and applications' (Wiley, 1974)

20 Di Bernardo, M., Budd, C., Champneys, A., Kowalczyk, P.: 'Piecewise-smooth dynamical systems, theory and applications' (Springer-Verlag, 2008)

21 Bizzarri, F., Brambilla, A., Storti Gajani, G.: 'Periodic small signal analysis of a wide class of type-ii phase locked loops through an exhaustive variational model', *IEEE Trans. Circuits Syst. I, Regul. Pap.*, 2012, **59**, pp. 2221–2231

22 Privault, N.: 'Stochastic analysis in discrete and continuous settings' (Springer, 2009)

23 Kundert, K.: 'Predicting the phase noise and jitter of PLL-based frequency synthesizers' (Designers Guide Consulting, Inc., 2006)

24 Thomson, D.: 'Spectrum estimation and harmonic analysis', *Proc. IEEE*, 1982, **70**, (9), pp. 1055–1096

25 Plaszczynski, S.: 'Generating long streams of $1/f^{\alpha}$ noise', *Fluct. Noise Lett.*, 2007, **7**, (1), pp. 1–13

26 Barnes, J.A.: 'Large sample simulation of flicker noise'. Proc. of Nineteenth Annual Precise Time and Time Interval (PTTI) Applications and Planning Meeting, December 1987, pp. 1–3

27 Greenhall, C.A.: 'Initializing a flicker-noise generator', *IEEE Trans. Instrum. Meas.*, 1986, **35**, (2), pp. 222–224

28 Biggio, M., Bizzarri, F., Brambilla, A., Carlini, G., Storace, M.: 'Reliable and efficient phase noise simulation of mixed-mode integer-*n* phase-locked loops'. European Conf. on Circuit Theory end Design, Dresden, September 8–12 2013

29 Brambilla, A., Linaro, D., Storace, M.: 'Nonlinear behavioural model of charge pump PLLs', *Int. J. Circuit Theory Appl.*, 2013, **41**, (10), pp. 1027–1046. [Online]. Available: http://dx.doi.org/10.1002/cta.1813

30 Chua, L., Desoer, C.A., Kuh, E.S.: 'Linear and nonlinear circuits' (McGraw-Hill, 1987)

31 Wanner, G., Hairer, E.: 'Solving ordinary differential equations II' (Springer-Verlag, 1991), vol. 1

32 Aprille, T., Trick, T.: 'A computer algorithm to determine the steady-state response of nonlinear oscillators', *IEEE Trans. Circuit Theory*, 1972, **19**, (4), pp. 354–360

33 Aprille, T., Trick, T.: 'Steady-state analysis of nonlinear circuits with periodic inputs', *Proc. IEEE*, 1972, **60**, (1), pp. 108–114

34 Kuznetsov, Y.A.: 'Elements of applied bifurcation theory' (Springer-Verlag, 2004, 3rd ed.)

35 Demir, A., Roychowdhury, J.: 'Phase noise in oscillators: a unified theory and numerical methods for characterization', *IEEE Trans. Circuits Syst. I, Fundam. Theory Appl.*, 2000, **47**, (5), pp. 655–674

8 Appendix 1: MNA formulation and variational model

The well-known MNA yields the following set of equations

$$\boldsymbol{F}(\dot{\boldsymbol{v}}(t), \boldsymbol{v}(t), t) = \underbrace{\frac{\mathrm{d}\boldsymbol{q}(\boldsymbol{v}(t))}{\mathrm{d}t}}_{\boldsymbol{h}(\dot{\boldsymbol{v}}(t),\boldsymbol{v}(t))} + \imath(\boldsymbol{v}(t)) + \boldsymbol{A}\boldsymbol{u}(t) = \boldsymbol{0} \qquad (9)$$

where $\boldsymbol{0} \in \mathbb{R}^S$ is the null column vector, t is time, $\boldsymbol{v} \in \mathbb{R}^S$ is a vector of ground-referenced node voltages, $\boldsymbol{q}:\mathbb{R}^S \to \mathbb{R}^S$ and $\imath:\mathbb{R}^S \to \mathbb{R}^S$ are functions mapping $\boldsymbol{v}$ to vectors whose entries are, respectively, sums of capacitive charges and resistive currents at a node, $\boldsymbol{u} \in \mathbb{R}^U$ is a vector of given inputs, and $\boldsymbol{A} \in \mathbb{R}^{S\times U}$ is an incidence matrix reflecting the contribution of $\boldsymbol{u}$ on each one of the S nodal current balances (Formulation (9) holds if the circuit includes also inductors and components that are not voltage controlled. In this case, the entries of $\boldsymbol{q}$ are capacitive charges and inductive fluxes and the entries of $\boldsymbol{v}$ are ground-referenced node voltages and branch currents. In this paper, this case will be neglected since a transformation, based on the insertion of ideal transformers and gyrators [30] always exists, which allows one to properly reformulate the problem avoiding this situation.).

Equation (9) is a DAE, since, in general, it is not completely solvable for the derivatives of $\boldsymbol{v}(t)$. A smooth analogue circuit is *well-posed* if its MNA formulation leads to a semi-explicit index-1 DAE [31], where (i) it is possible to separate the dynamical variables (those appearing in (9) together with their time derivatives) from the algebraic ones, and (ii) the algebraic variables can be obtained from the dynamical ones by resorting to the implicit function theorem.

In the following, without lack of generality, (9) will be assumed to be an index-1 DAE. Since a given circuit admitting an index-1 DAE description can be transformed in an equivalent one admitting an ode description [30], we will focus on the ODE case.

The homogeneous linear time-varying system corresponding to linearisation of (9) around a solution $\boldsymbol{v}_s(t)$ can be

written as

$$\left[\underbrace{\left.\frac{\partial \boldsymbol{h}(\dot{\boldsymbol{v}},\boldsymbol{v})}{\partial \boldsymbol{v}}\right|_{\substack{\boldsymbol{v}(t)=\boldsymbol{v}_s(t)\\ \dot{\boldsymbol{v}}(t)=\dot{\boldsymbol{v}}_s(t)}}}_{\boldsymbol{B}(t)} + \underbrace{\left.\frac{\partial t}{\partial \boldsymbol{v}}\right|_{\substack{\boldsymbol{v}(t)=\boldsymbol{v}_s(t)\\ \dot{\boldsymbol{v}}(t)=\dot{\boldsymbol{v}}_s(t)}}}_{\boldsymbol{G}(t)}\right]\boldsymbol{\xi}(t) + \underbrace{\left.\frac{\partial \boldsymbol{h}(\dot{\boldsymbol{v}},\boldsymbol{v})}{\partial \dot{\boldsymbol{v}}}\right|_{\substack{\boldsymbol{v}(t)=\boldsymbol{v}_s(t)\\ \dot{\boldsymbol{v}}(t)=\dot{\boldsymbol{v}}_s(t)}}}_{\boldsymbol{C}(t)}\dot{\boldsymbol{\xi}}(t)=\boldsymbol{0} \tag{10}$$

where $\boldsymbol{\xi}(t)$ is a *small* perturbation whose evolution is computed with respect to $\boldsymbol{v}_s(t)$ from an initial condition $\boldsymbol{\xi}(t_0)=\boldsymbol{\xi}_0$. If all the capacitors of the circuit are linear, in (10) $\boldsymbol{C}(t)$ is a constant matrix and $\boldsymbol{B}(t)$ is a null matrix. Since it has been assumed that (9) is an ode, $\boldsymbol{C}(t)$ is not singular and it is then possible to recast (10) as

$$\dot{\boldsymbol{\xi}}(t)=\underbrace{-\boldsymbol{C}^{-1}(t)[\boldsymbol{B}(t)+\boldsymbol{G}(t)]}_{\boldsymbol{J}(t)}\boldsymbol{\xi}(t) \tag{11}$$

In general, (11) is solved in parallel with (9), since its solution provides the time evolution of the fundamental transition matrix $\boldsymbol{\Phi}_{\boldsymbol{v}_0}(t,t_0)$. One has then to solve the extended problem

$$\begin{cases} \boldsymbol{h}(\dot{\boldsymbol{v}}(t),\boldsymbol{v}(t))+\imath(\boldsymbol{v}(t))+\boldsymbol{A}\boldsymbol{u}(t)=\boldsymbol{0} \\ \dot{\boldsymbol{\Phi}}_{\boldsymbol{v}_0}(t,t_0)=\boldsymbol{J}(t)\boldsymbol{\Phi}_{\boldsymbol{v}_0}(t,t_0) \\ \boldsymbol{v}(t_0)=\boldsymbol{v}_0 \\ \boldsymbol{\Phi}_{\boldsymbol{v}_0}(t_0,t_0)=\boldsymbol{1}_S \end{cases} \tag{12}$$

where $\boldsymbol{1}_S$ is the $S\times S$ identity matrix. For instance, if the circuit admits a T-periodic steady-state solution Ω and one is able to find an initial condition $\boldsymbol{v}_0$ belonging to Ω (usually this is done in time domain by shooting methods [32, 33]), the solution of (12) provides the monodromy matrix $\boldsymbol{\Phi}_{\boldsymbol{v}_0}(T+t_0,t_0)$ whose eigenvalues (the Floquet multipliers) can be used to study the stability of Ω [34]. Moreover, the numerical evaluation of $\boldsymbol{\Phi}_{\boldsymbol{v}_0}(t,t_0)$ is crucial whenever one is interested in periodic small-signal analysis (PAC) and PNOISE or to compute phase noise in oscillators [35].